RSC Advances

PAPER

View Article Online
View Journal | View Issue

Cite this: *RSC Adv.*, 2023, **13**, 31622

A density functional theory study on the adsorption of different organic sulfides on boron nitride nanosheet†

Zhengjian Hou,‡[a] Xufeng Lin,‡*[ab] Ke Wu,[c] Hua Chi,[a] Wumin Zhang,[a] Lishuang Ma*[a] and Yanyan Xi[d]

The adsorption of methanethiol (**MT**), thiophene (**T**), benzothiophene (**BT**), dibenzothiophene (**DBT**) on hexagonal boron nitride (**h-BN**) has been investigated by the framework of the density functional theory (DFT) calculations in this work. The prefer adsorption sites and interfacial angles of different sulfur compounds on the surface of the **h-BN** are investigated and analyzed. The adsorption energy results indicated that the adsorption of **MT** (E_{ad} ≈ −6 kcal mol^{-1}), **T** (E_{ad} ≈ −10 kcal mol^{-1}), **BT** (E_{ad} ≈ −15 kcal mol^{-1}), and **DBT** (E_{ad} ≈ −21 kcal mol^{-1}) on monolayer **h-BN** is physical interaction, and the value of E_{ad} on bilayer **h-BN** is more than that on monolayer **h-BN** 0.05%. Adsorptive conformations show that sulfides prefer to be adsorbed on center B atoms rather than N atoms. Meanwhile, thiophene and its analogues tend to be adsorbed parallel on **h-BN** plane. Energy decomposition, natural population analysis (NPA), and electrostatic potential (ESP) analysis used to better understand the nature of adsorption on **h-BN**. van der Waals force plays a dominant role in adsorption process. Due to the π–π interactions, **T**, **BT**, and **DBT** have larger van der Waals forces than **MT** and the value of adsorption energy is negative correlated to the number of benzene rings. These findings are helpful for deeper understanding the adsorptive desulfurization mechanism and help develop better adsorbents for desulfurization in the future.

Received 22nd August 2023
Accepted 23rd October 2023

DOI: 10.1039/d3ra05718f

rsc.li/rsc-advances

1. Introduction

Ultra-deep desulfurization of commercial fuel is of growing concern nowadays. The sulfur (*S*)-containing species in oil are not only harmful to environmental livings, but also poisonous for metal-based catalysts in the oil-refining and petrochemical processes. Therefore, many researchers are devoted to reduce the S content in fuel,[1–3] and the present desulfurization methods includes hydrodesulfurization (HDS),[4] oxidative desulfurization (ODS),[5,6] extraction desulfurization,[7] bio-desulfurization (BDS)[8] and adsorptive desulfurization (ADS).[9–12] Among them, ADS has attracted extensive attentions especially for ultra-low S oils because of its mild process conditions and low operation cost.

Up to now, several types of adsorbent have been successfully applied for ADS, such as metal oxides,[13,14] zeolites,[15–17] activated carbons,[18] metal organic frameworks (MOF),[19,20] boron nitride (BN)[21–23] including hexagonal boron nitride (**h-BN**)[24,25] and so on. BN-based materials in general, like their carbon-based analogues, can existed in various nanostructures including nanotubes,[23] nanosheets,[26] nanobowls,[27] are potentially useful materials in the field of adsorbent–adsorbate interactions like pollutant removal and drug delivery. In particular, the **h-BN**-based adsorbents have gained particular attentions because of its unique layer–structure properties, high specific surface area, remarkable durability and adsorption capacity. These characteristics make **h-BN** become a promising carrier for dispersion of active species.[1,4] Li *et al.*[28] introduced Sn-based deep eutectic solvents (DESs) into **h-BN** to obtain superior adsorption performance. Sn-BN showed an adsorption capacity of 17.93 mg S g^{-1}. Sun *et al.*[29] prepared the Cu-intercalated layered **h-BN**/N-doped carbon-nanofiber composite films (PAN-Cu/ABN-CNFs). Its adsorption capacity was up to 78.38 mg S g^{-1} and the adsorption capacity after a four-time regeneration recycling still maintained at 74.894 mg S g^{-1}. In short, **h-BN** is a promising adsorbent for ADS and it is of great importance to study its adsorption mechanism to further improve its performance.

[a]*College of Chemistry and Chemical Engineering, China University of Petroleum (East China), Qingdao 266580, China. E-mail: hatrick2009@upc.edu.cn; hxmals@upc.edu.cn; Tel: +86-532-86981975*

[b]*State Key Laboratory of Heavy Oil Processing, China University of Petroleum (East China), Qingdao 266580, China*

[c]*Changqing Engineering Design Co. Ltd., PetroChina Changqing Oilfield Company, Xi'an 710000, Shanxi, China*

[d]*Advanced Chemical Engineering and Energy Materials Research Center, China University of Petroleum (East China), Qingdao 266580, China*

† Electronic supplementary information (ESI) available. See DOI: https://doi.org/10.1039/d3ra05718f

‡ These two authors contribute equally to this paper.

However, it is difficult to study the adsorption mechanisms and active sites through experimental method due to high costs. In contrast, computational chemistry provides powerful tools for investigating adsorption mechanism. For example, Li *et al.*[30] investigated the dibenzothiophene (**DBT**) adsorption strength on the pristine and O-doped **h-BN** monolayer by density functional theory (DFT) calculations. Larijani *et al.* studied the adsorption of glycine amino acid and its zwitterionic form on graphene, **h-BN** and silicon carbide (h-SiC).[31] The interaction of sulfur mustard, a chemical warfare agent, with the surface of C_{24}, $C_{12}Si_{12}$, $Al_{12}N_{12}$, $Al_{12}P_{12}$, $Be_{12}O_{12}$, $B_{12}N_{12}$ and $Mg_{12}O_{12}$ nanocages was studied using the dispersion corrected density functional theory (DFT-D3) method.[32] In addition, Xiong *et al.* found that the strong interaction between **DBT** and the graphene-like BN or BN nanowire came from the occupied π-electrons of the B atoms orbitals.[22] The driven force for adsorption of aromatic compounds on **h-BN** is qualitatively proposed to be π–π interaction.[33]

Modified **h-BN** and other adsorbents are often used to adsorb only one sulfide according to previous researches. However, there are many different sulfur compounds needs to be adsorbed and separated in reality. The study on adsorption behaviors of different molecules has a significant effect on separation and purification in chemical engineering, as well as in molecular recognition.[33] For example, CO and CO_2 are recovered from blast furnace exhaust gas, BZ and **DBT** are separated and removed in petrochemical industry. Therefore, it is necessary to study the adsorption mechanisms of adsorbents for different sulfur compounds. Though the adsorptive energies of several sulfurs on **h-BN** and graphene were previously studied, the comprehensive analyses of the interaction nature between the adsorbates and adsorbents are still inadequate.

In this work, adsorption mechanisms of different sulfur compounds adsorbed on the surface of model **h-BN** sheets were investigated through the density functional theory (DFT). A series adsorption model of sulfur compounds adsorbed on **h-BN** with different sites and interfacial angles was obtained and optimized.[34] The adsorption energy (E_{ads}) of different structures were compared and the mechanism of ADS was analyzed.

2. Computational methods

DFT calculations including the Grimme's D3 dispersion correction (DFT-D3BJ) were performed using the Gaussian 09 program suite[35] to investigate the adsorption mechanism of various sulfur compounds on the **h-BN**. All geometries including the sulfur compounds, **h-BN**, as well as their adsorption complexes were fully optimized using the B3LYP-D3BJ functional with the 6-31G(d,p) basis set. Vibrational frequency analyses were also performed at the same level of theory to confirm that the obtained structures are true minima with no imaginary frequencies. The B3LYP functional had been demonstrated to be a reliable commonly used theoretical level for studying adsorption of different nanostructures.[36–39] It has proven that the B3LYP/6-31G(d,p) is a suitable theoretical method for medium systems to provide acceptable results with low cost.[39] To avoid the underestimation of the interaction between sulfur compound and BN nanosheet due to dispersion problem,[40,41] the D3BJ dispersion correction was applied for all DFT calculations.[42]

The model S compounds studied in this work include methanethiol (**MT**), thiophene (**T**), benzothiophene (**BT**), and dibenzothiophene (**DBT**). To represent the **h-BN** sheet, a slab of hexagonal lattice composed of 27B and 27N atoms were constructed, where the dangling bonds were saturated with hydrogen atoms to minimize the edge effect. The global charge of the model S compounds, the model **h-BN** sheet, and their adsorption systems are zero. The spin multiplicity of them are 1 since all S compounds have closed-shell electronic configuration, and the model **h-BN** sheet has a singlet ground state compared to its triplet state.

The adsorption energy (E_{ad}) was calculated as follows,

$$E_{ad} = E_{sulfur/BN} - E_{BN} - E_{sulfur} + E_{BSSE} \quad (1)$$

where the $E_{sulfur/BN}$ is the total energy of the adsorbed origin sulfide molecules on **h-BN** nanosheet. E_{sulfur} and E_{BN} represent the energies of the isolated sulfur molecules (**MT**, **T**, **BT** and **DBT**) and the individual BN sheet, respectively. Zero-point energy (ZPE) corrections were obtained from the vibrational frequency analysis, and the ZPE corrected electronic energies were used for $E_{sulfur/BN}$, E_{sulfur} and E_{BN}. E_{BSSE} is the basis set superposition error (BSSE) for the adsorption energy calculated by the counter-poise method.[43] Energy decomposition analysis is performed on PSI4, natural population analysis (NPA) on Gaussian 09, electrostatic potential (ESP) on GaussView 6.[44–46]

In order to further support the rationality of the basis set as well as the B3LYP-D3BJ method used in this work, the E_{ad} of **MT** adsorbed on the above described $B_{27}N_{27}$ sheet (with η^1 conformation, *vide infra*) using the 6-31G(d,p) basis sets was compared to that using the 6-311G(d,p) basis set. The small error (0.7 kcal mol^{-1}, see first two line of Table S1 in the ESI†) supports the rationality of using the 6-31G(d,p) basis sets for description of the adsorption system interested in this work. Furthermore, a benchmark calculation on the E_{ad} of **MT** on a B_3N_3 ring was also carried out with the results being collected in Table S2.† From Table S2† it can be seen the presently used B3LYP-D3BJ/6-31G(d,p) level predicts a rather close E_{ad} compared to another popular method of M06-2X-D3. More importantly, B3LYP-D3BJ/6-31G(d,p) also predicts a quite close E_{ad} compared to post-SCF levels of MP2/AGU-CC-PVDZ, with the error of less than 1.0 kcal mol^{-1}. These comparisons show that using B3LYP-D3BJ method is appropriate for studying the adsorption systems interested in this work.

3. Results and discussion

3.1 Adsorptive conformations and energies of the sulfides on a monolayer h-BN sheet

In this section, the adsorption conformations and energies of the sulfur adsorbates on the monolayer **h-BN**, as well as the influence of different possible adsorptive sites are discussed. Fig. 1a shows the optimized structure of a slab of hexagonal lattice composed of 27B and 27N atoms. The $B_{27}N_{27}$ sheet was

selected to represent the **h-BN** monolayer, which has been proven to be reliable to study the adsorption performance of **h-BN** nanosheets toward various adsorbates.[33] The interested sulfur adsorbates in this work, including methanethiol (**MT**), thiophene (**T**), benzothiophene (**BT**), and dibenzothiophene (**DBT**), are also shown in Panels b–e in Fig. 1.

As the **h-BN** sheet has a polar surface with non-uniform charge distribution due to the difference in the polarity of B and N, the **h-BN** sheet can offer more differentiated adsorptive sites than the graphene sheet. On a given **h-BN** monolayer, the electronegative sulfur ad-atoms can interact with BN surface either through a point-to-point site of an electropositive B atom (denoted as η^1:B-site) or through an on-top site of a six-membered B_3N_3 ring (denoted as η^6-site). In addition, the π–π stacking interaction cannot be ignored for the aromatic sulfur adsorbates. By taking the above factors into consideration, the stable adsorptive conformations were obtained as illustrated in Fig. 2–4. Note that all these conformations were fully optimized without any structural restrictions. Hereafter in this paper, the notation of **XX/h-BN** (where **XX** represent a certain adsorbate of **MT**, **T**, **BT** or **DBT**) is used to represent the adsorption complexes of different sulfides on an **h-BN** sheet. A suffix of "-mono" or "-bi" represents the **h-BN** sheet is a monolayer or bilayer one. This paper mainly contains the result of a monolayer **h-BN** sheet (except Section 3.2), so when no suffix was used, the notation refers to the monolayer case. A suffix of "-η^n" (where $n = 1$, 2 and 6 in this work) represent different type of adsorption conformation for a certain adsorption system. For example, the notation of **MT/h-BN**-η^n ($n = 1$, 2 and 6 in this work) is used to define the adsorption complex where the **MT** occupies the η^n site, and the η^1 below will specifically represent the η^1:B-site.

The calculated results show that two most stable conformations of **MT/h-BN** in which the sulfur atom located at the η^1:B-site and the η^6-site of **h-BN** exhibit close adsorption energies, *i.e.* −5.8 and −6.0 kcal mol^{-1} respectively (see Table 1). This suggests that the η^6-site and the η^1:B site may compete in stabilizing the sulfide/**h-BN** complex. As can be seen from the geometry parameters shown in Fig. 2, the equilibrium distance from the S atom to the hexagonal BN plane in the **MT/h-BN**-η^1 complex is 3.307 Å, and meanwhile the geometry parameters (bond length and bond angles) of the complex remained almost unchanged compared with the individual **MT** and **h-BN**, which indicates the non-covalent physisorption characteristic between the two entities. The **MT/h-BN**-η^6 complex shows a physisorption conformation since the B–S distances between the S atom and the closest BN hexagon vary in the range of 3.47–3.95 Å, and the S–N distances are in the range of 3.40–3.88 Å.

Table 1 Effects of different sites and degrees on adsorption energy values of XX/h-BN system (where XX = MT, T, BT and DBT)

Species	Adsorptive site	Interfacial angles	E_{ad} (kcal mol^{-1})
MT/h-BN	η^1	—	−5.8
	η^6	—	−6.0
T/h-BN	η^1	0	−10.1
	η^1	15	0.4
	η^1	60	0.5
	η^1	90	1.1
	η^6	0	−10.1
BT/h-BN	η^1	0	−15.7
	η^6	0	−15.0
DBT/h-BN	η^1	0	−21.3
	η^6	0	−21.3

Since in practice ADS is often carried out in oil like gasoline or diesel, the E_{ad} of **MT** on the **BN** sheet with gas phase model was compared to the those with the solvation models using *n*-heptane (representing gasoline) and using *n*-dodecane (representing diesel). The E_{ad} with the gas phase model (the 1st entry in Table S1†) is quite close to those of the solvation model (the 3rd and 4th entries in Table S1†), showing in these ADS systems oil solvents play trivial roles. On the other hand, besides the adsorption of **MT** on the central BN ring in the $B_{27}N_{27}$ model (Fig. 2a), the possible edge effect was also investigated by comparing the E_{ad} of **MT** on different sites with η^1 conformation (Fig. S1 in ESI†). The E_{ad} results listed in Table S1† show

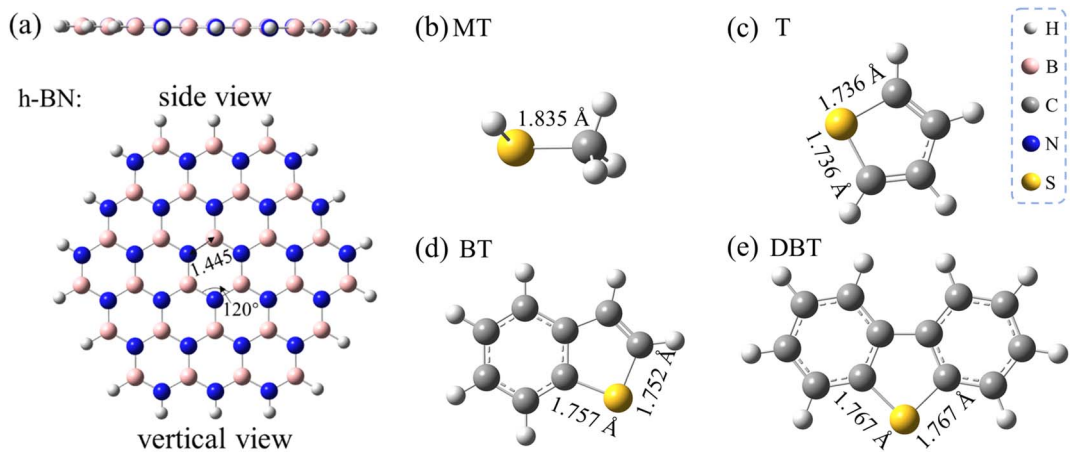

Fig. 1 Optimized geometries of **h-BN** monolayer and sulfur adsorbates studied in this work. (a) The monolayer BN sheet model, (b) **MT**, (c) **T**, (d) **BT**, and (e) **DBT**. All distances are indicated in angstroms.

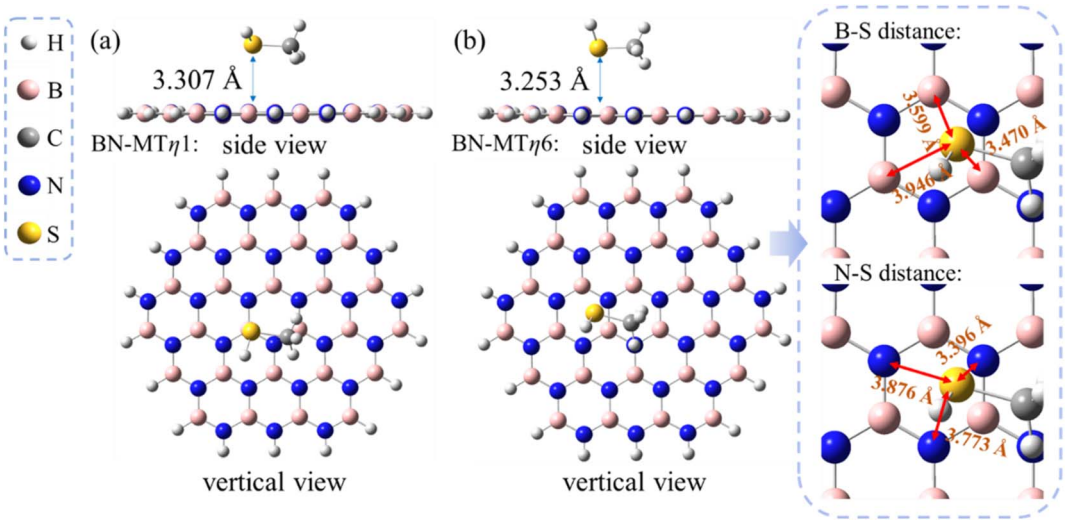

Fig. 2 Optimized geometries of methanethiol (MT) adsorbates on h-BN monolayer. (a) Side and vertical view of MT/h-BN-η^1. (b) Side and vertical view of MT/h-BN-η^6. Inset: zoom in for the structure of adsorption sites. All distances are indicated in angstroms.

that the E_{ad} values are quite close for these different sites. Therefore, the solvation effect and edge effect on the adsorption behavior and energy were no longer considered for other adsorption systems in this work.

Besides the aliphatic methanthiol **MT**, the aromatic sulfur compounds such as **T**, **BT** and **DBT** adsorbates were also investigated, in order to explore the influence of the π–π interaction during the ADS process. For this purpose, we first performed a series of optimizations by fixing the interfacial angle (Φ) between **T** and **h-BN** from 15° to 90°, and the B–S distances being fixed at 3.30 Å (panels a–d in Fig. 3). As shown in Table 1, the adsorption strength gradually decreases as the dihedral angle Φ increases and the π–π interaction strength decreases. These changes indicate that the π–π interaction plays an important role in the ADS process. It is worth noting that the adsorption energy of **T/h-BN**-η^1 with Φ = 90° (−4.8 kcal mol^{-1}) is smaller than that of **MT/h-BN**-η^1 (−5.8 kcal mol^{-1}), partly due to the weaker electronegativity of sulfur atom on **T** than **MT**. When global optimization was performed for the **T/h-BN** complex without any constraints, three

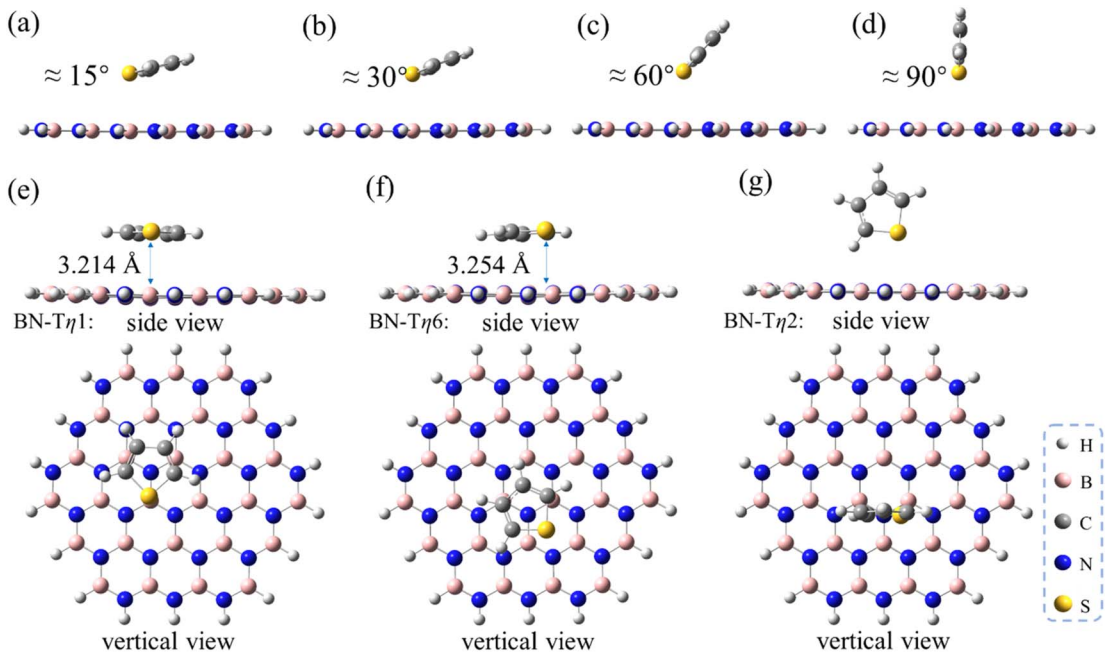

Fig. 3 Optimized structures of T/h-BN with different adsorption conformations. (a–d) The interfacial angel of adsorbate and adsorbent molecules fixed at different angels as indicated. (e–g) Optimized geometries of the -η^1, -η^6 and -η^2 sites, respectively. All distances are indicated in angstroms.

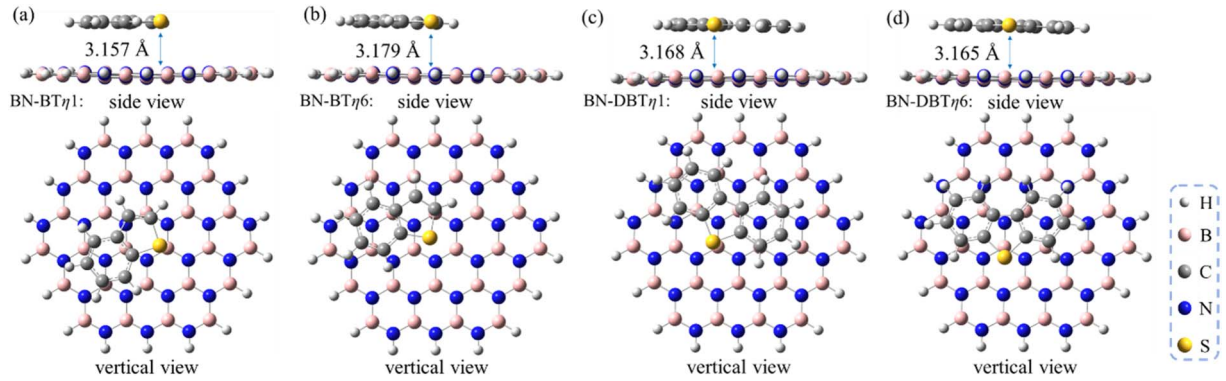

Fig. 4 Optimized structures of (a) BT/h-BN-η^1, (b) BT/h-BN-η^6, (c) DBT/h-BN-η^1 and (d) DBT/h-BN-η^6. All distances are indicated in angstroms.

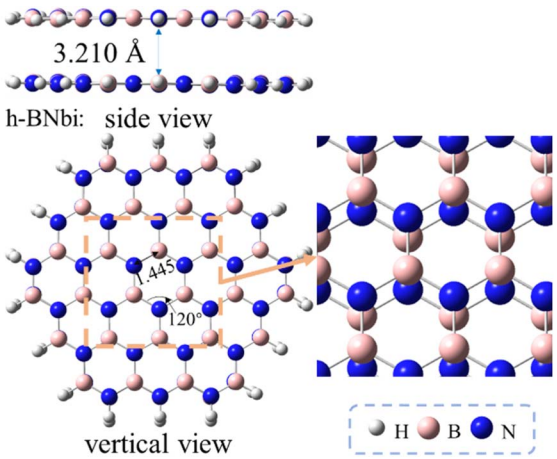

Fig. 5 Optimized structures of a bilayer h-BN sheet.

Table 2 Effects of different sites on adsorption energy values of XX/h-BN-bi system (XX = MT, T, BT and DBT)

Species	Adsorptive site	E_{ad} (kcal mol^{-1})
MT/h-BN-bi	η^1	−6.3
	η^6	−6.3
T/h-BN-bi	η^1	−10.8
	η^6	−10.6
BT/h-BN-bi	η^1	−16.6
	η^6	−15.9
DBT/h-BN-bi	η^1	−22.6
	η^6	−22.6

energy minima were obtained including **T/h-BN**-η^1, **T/h-BN**-η^6 and **T/h-BN**-η^2 as shown in panels e–g in Fig. 3. The calculated results show that the **T/h-BN**-η^2 structure with a perpendicular orientation has an adsorption energy of −6.7 kcal mol^{-1}, which is obviously lower than that of the **T/h-BN**-η^1 structure with Φ = 90°. Not surprisingly, the π–π stacked **T/h-BN**-η^1 and the **T/h-BN**-η^6 conformations exhibit similar stabilities with low adsorption energies (−10.06 and −10.07 kcal mol^{-1}). These calculated results indicate that the π–π stacking interaction plays an important role in the ADS process on the **h-BN** adsorbent.

To further evaluate the influence of the strength of π–π interaction on stabling the sulfur/**h-BN** complex, the **BT** and **DBT** adsorbates having two and three aromatic rings, respectively, were also studied. It was found that on the one hand, the π–π stacked η^1-site- and η^6-site-adsorptive conformations are also the two most energetically favorable ones with similar adsorption energies for the cases of **BT** and **DBT** adsorbates (Fig. 4). On the other hand, the adsorption energy increase with the order of **MT** < **T** < **BT** < **DBT**, ranging from −6.0 to −21.4 kcal mol^{-1} (Table 1). In addition, the distances between all sulfides and BN plane become closer around 3.2–3.3 Å (see geometries of adsorbed **MT**, **T**, **BT** and **DBT** shown in Fig. 1–4). This suggests that the more aromatic the sulfide is, the significantly stronger the adsorption interaction will be.

3.2 Adsorptive conformations and energies of the sulfides on a bilayer h-BN sheet

In this section, the adsorptive conformations and energies of the sulfides on bilayer **h-BN** was explored to understand the effect of BN layer stacking on adsorption desulfurization performance. As shown in Fig. 5, the so-called AA′ stacking conformation, where the B atoms on lower layer are eclipsed by the N atoms on upper layer and *vice versa*, has been reported to be the most favorable pattern among the five possible ones, *i.e.* AA, AA′, AB, AB′ and A′B, for a bilayer **h-BN** sheet.[47] So the AA′-stacked bilayer **h-BN** was considered as the other interested adsorbent in this paper. The formation energy of this bilayer **h-BN** was calculated to be −96.3 kcal mol^{-1} by using the following formula,

$$E_{form} = E_{bilayer} - 2E_{monolayer} \quad (2)$$

The adsorptive conformations systematically become more stabilized with the order of **MT**, **T**, **BT** and **DBT**, similar as the results of monolayer **h-BN** case (Table 2 compared to Table 1). The adsorption energies are ranged from −6.0 to −21.4 kcal mol^{-1} which is also same as the results of monolayer **h-BN**. Therefore, π–π effects also plays an important role in

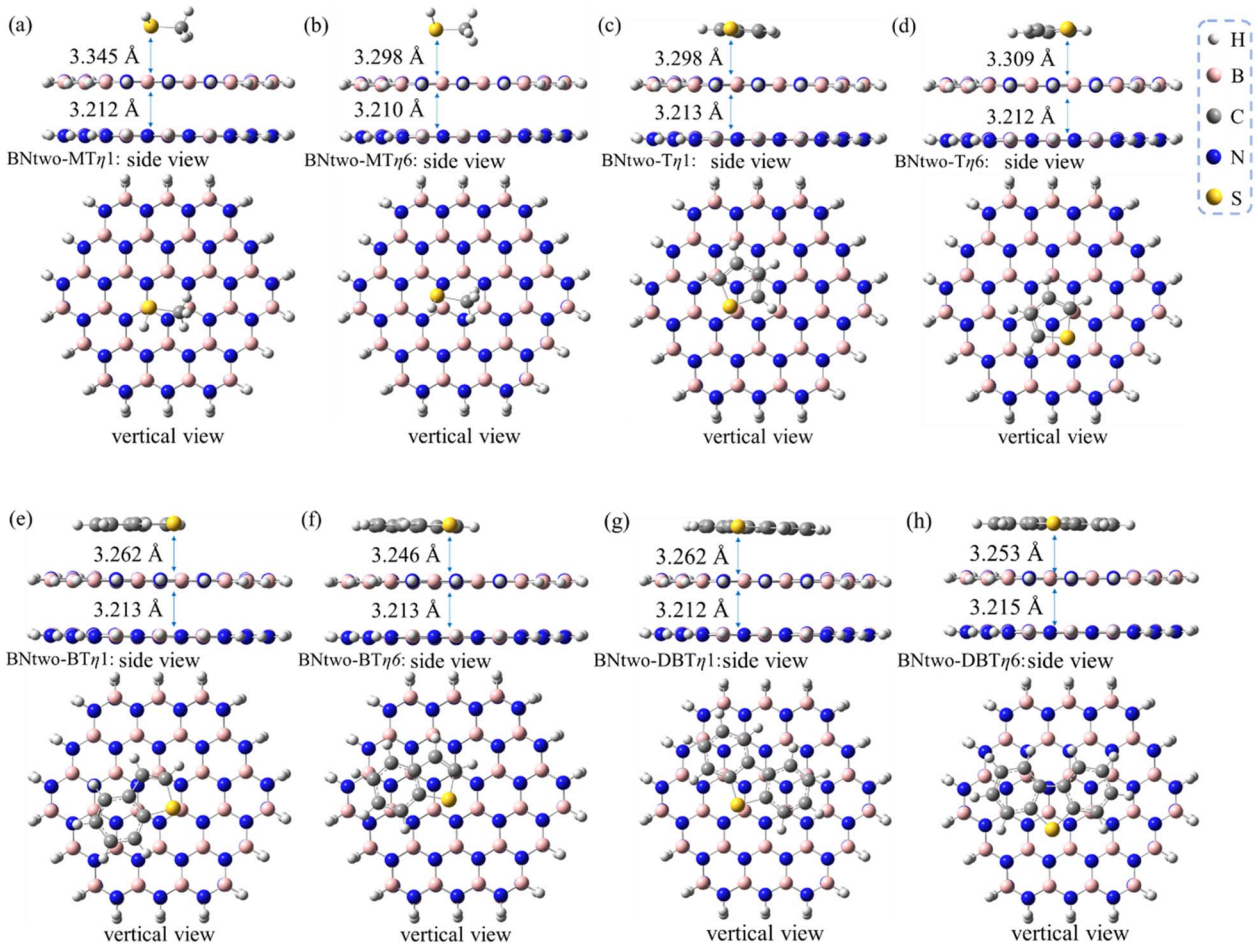

Fig. 6 Optimized structures of (a) MT/h-BN-bi-η^1, (b) MT/h-BN-bi-η^6, (c) T/h-BN-bi-η^1, (d) T/h-BN-bi-η^6, (e) BT/h-BN-bi-η^1, (f) BT/h-BN-bi-η^6, (g) DBT/h-BN-bi-η^1, and (h) DBT/h-BN-bi-η^6. All distances are indicated in angstroms.

Table 3 The distance (*d*) from the adsorbed sulfides to the h-BN plane for the sulfide adsorption systems involving a monolayer and a bilayer h-BN sheet, respectively

Species	Adsorption conformation	$d_{monolayer}$ (Å)	$d_{bilayer}$ (Å)
MT/h-BN	η^1	3.307	3.345
	η^6	3.253	3.298
T/h-BN	η^1	3.214	3.298
	η^6	3.254	3.309
BT/h-BN	η^1	3.157	3.262
	η^6	3.179	3.246
DBT/h-BN	η^1	3.168	3.262
	η^6	3.165	3.253

bilayer systems. Meanwhile, there are also two competitive adsorptive conformations (η^1 and η^6) for the bilayer **h-BN** systems (see Fig. 6). The distance from sulfides to bilayer **h-BN** is slightly larger than that of the monolayer case (Table 3), indicating a second **h-BN** layer has a weakening effect for the sulfide adsorption on the **h-BN** adsorbents.

3.3 Further analysis for the nature of adsorption on h-BN

3.3.1 Energy decomposition analysis. Fig. 7 shows the results of energies decomposition of the sulfide adsorption systems using symmetry adapted perturbation theory (SAPT). Electrostatics, exchange-repulsion, induction, dispersion contributions and total SAPT are included.[48,49] The results of total SAPT energy shows that **MT/h-BN** has the highest energy, **DBT/h-BN** has the lowest (Fig. 7a). Generally, the energy value and order are consistent with calculated E_{ad} results (Tables 1 and 2).

The electrostatics and dispersion effect contribute the most to the interaction among four interactions. Dispersion effect dominates in the adsorption system, and electrostatics is smaller. Therefore, electrostatics and dispersion play main role in the adsorption system studied above, and are discussed in the following part. The electrostatics effect comes from the positive and negative charges in adsorption system, and the dispersion effect comes from the weak van der Waals force and π–π interaction.

Both electrostatics and dispersion energy increase as the adsorbate changing from **MT** to **DBT**, and the dispersion increases more. On the one hand, the negative charge of S atom

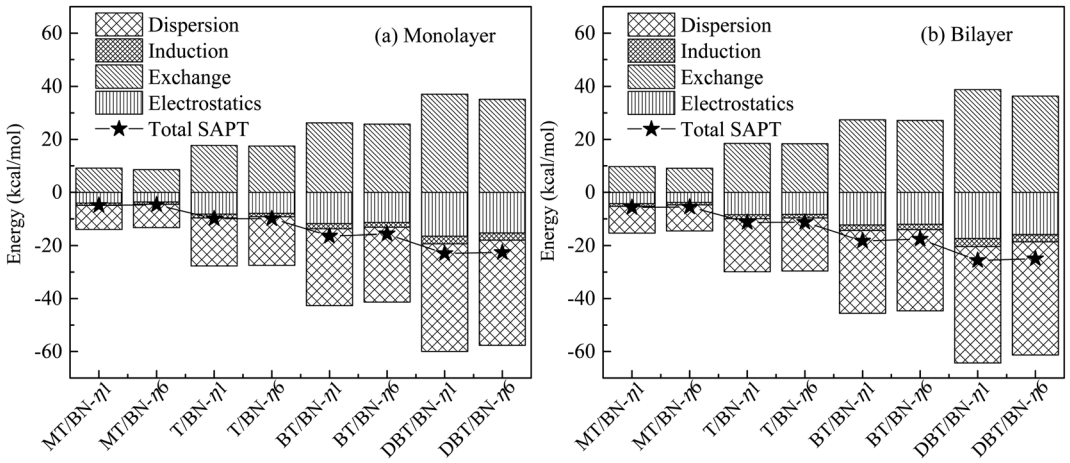

Fig. 7 Symmetry adapted perturbation theory (SAPT) energy decomposition of (a) sulfide/**h-BN-mono** and (b) **sulfide/h-BN-bi** adsorption systems, where, sulfide represents one of **MT**, **T**, **BT** or **DBT**.

is partly dispersed due to the aromatic properties in sulfides. Thus the negative region contacting with **h-BN** plane increases. Accordingly, the electrostatic effect increases. For example, the charge of C and H on **DBT** is more negative than that on **MT** because of conjugation. Otherwise, it can be concluded that electrostatics of η^1 is stronger than η^6. This may be due to the negative charge center of S atom is closer to B atom in η^1, and the charge effect is stronger. On the other hand, lager adsorbate could result in increasing van der Waals force (dispersion force). In addition, the aromatic ring on adsorbate will form π–π mode with the six-membered ring on **h-BN**, which further strengthens the van der Waals force.

Therefore, the adsorption of **T**, **BT** and **DBT** on **h-BN** is stronger than **MT**, and the effect mainly attribute to dispersion and electrostatics. The π–π interaction between sulfides and **h-BN** will increase with more benzene rings. The monolayer and bilayer of **h-BN** adsorption systems have the same properties.

3.3.2 Natural population analysis (NPA) charge. NPA can provide information about charge transfer and distribution. It is found that the ΔQ (e) of all cases are negative in monolayer **h-BN**, showing that electron transfer occurs from S to **h-BN** (Table 3).[30] The charge translocations are calculated to be systematically increased from the case of **MT** to **DBT**. Especially, sulfides adsorbed on η^6 site has less charge transfer than on η^1 site. The reason may be due to that the distance between S and B in η^6 is longer than that in η^1.

The results above are in line with the adsorption energies (the E_{ad} decrease in order **MT**, **T**, **BT** and **DBT**) as well as the stabilities of the sulfur/**h-BN** complexes. While the charge transfers are both below 0.05e, indicating that the charge effect is not strong. And it is similar to electrostatics in the energy decomposition analysis. The results of bilayer **h-BN** system are consistent with the monolayer system.

3.3.3 Electrostatic potential surfaces analysis. Electrostatic potential (ESP) analysis is introduced to analyze non-covalent interaction systems in this work. Four stable adsorption conformations (**MT/h-BN**, **T/h-BN**, **BT/h-BN** and **DBT/h-BN**) were analyzed by ESP (Fig. 8) calculation. It can be seen that on the ESP surface, electrostatic potential value is negative in the red area, which is easy to give electrons, and the electrostatic potential value is positive in the blue area, which is easy to obtain electrons.[1,30] For example, the H atom of the edge B–H group in **h-BN**, sulfur atom (in **MT**/**h-BN**) are negatively charged region, while the H atom of the edge N–H group in **h-BN** and C–H group in sulfides are positively charged region (Fig. 8a). It can be concluded that the negatively charged region (around the S atom) of sulfides will be close to the positively charged region (around the B atom) of **h-BN**, resulting in the formation of η^1 site. In contrast, there is no structure in which negatively charged S atom is adsorbed on N atom with same negatively charge. Besides, η^6 is a special adsorption site (Fig. 8b). The adsorption site is in the middle of the six-membered ring where the charge density is relatively small, but its stability is the same as η^1. It also indicates that the charge effect in the system is not the dominant one, which is consistent with the results of energy decomposition analysis (Table 4).

The negative charge on S atom is dispersed due to the existence of large conjugate structure (panels c–h in Fig. 8). Whereas S atom is still the center where the negative charge of sulfide is concentrated to interact with B atom. As a result, the adsorption sites of **T**, **BT** and **DBT** are the same as **MT**. It can be seen from Fig. 8 that the adsorption area of **DBT** and the negatively charged area of the system are the largest one. This is the reason why the value of adsorption energy of **DBT** on **h-BN** is most negative among four sulfides.

4. Conclusions

In summary, the adsorption behavior and nature of four S-containing compounds on model **h-BN** nanosheets were systematically investigated with DFT calculations. Primary conclusions can be drawn as follows.

(i) Sulfides can be adsorbed on **h-BN** with two energetically competitive conformations, namely point-to-point (η^1, through S···B interaction) and point-to-ring-center (η^6) ones. The plane

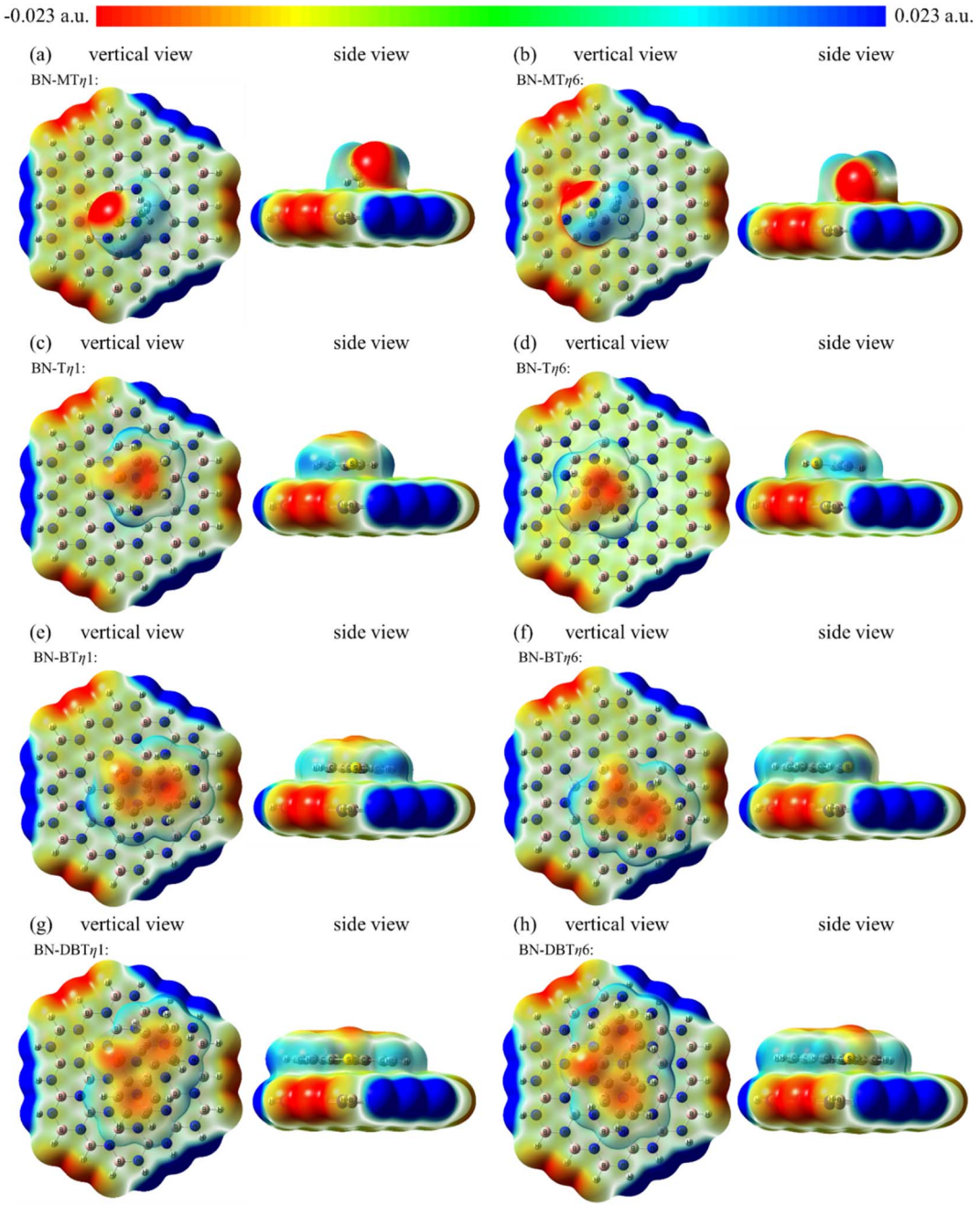

Fig. 8 Electrostatic potential surfaces of (a) MT/h-BN-mono-η^1, (b) MT/h-BN-mono-η^6, (c) T/h-BN-mono-η^1, (d) T/h-BN-mono-η^6, (e) BT/h-BN-mono-η^1, (f) BT/h-BN-mono-η^6, (g) DBT/h-BN-mono-η^1, and (h) DBT/h-BN-mono-η^6 mapped on electron total density (isoval = 0.0004).

of **T**, **BT** or **DBT** tends to be adsorbed parallel on **h-BN** plane. Besides, the adsorption energies increase with the order of **MT** < **T** < **BT** < **DBT**. There rules are feasible for both of the monolayer and bilayer **h-BN** cases.

(ii) Electrostatic effects, the interactions between positive and negative charges, play an important role in the adsorption process. The S atom tends to adsorbed near to the positively charged B atom. Therefore, electrostatic effect in the conformation η^1, where negative center of sulfide S atom is closer to the B atom, is stronger than that of η^6.

(iii) van der Waals force plays a dominant role in adsorption process. Compared with the case of **MT**, the π–π interaction of **T**, **BT** and **DBT** with **h-BN** strengthens the van der Waals force. This effect increases with increasing number of benzene rings in the adsorbate.

The above findings provide deeper understandings about sulfides adsorption mechanism on BN type absorbents in particular, and on wider types of absorbents in general. The new understandings may help design better adsorbent for adsorptive desulfurization in the future.

Table 4 NPA charges transferred from sulfide to h-BN for different adsorption systems

Structure	Adsorption conformation	ΔQ (e)	
		h-BN	Adsorbate
MT/h-BN-mono	η^1	−0.018	0.018
	η^6	−0.009	0.009
T/h-BN-mono	η^1	−0.029	0.029
	η^6	−0.026	0.026
BT/h-BN-mono	η^1	−0.034	0.034
	η^6	−0.031	−0.031
DBT/h-BN-mono	η^1	−0.044	0.044
	η^6	−0.034	0.034
MT/h-BN-bi	η^1	−0.022	0.022
	η^6	−0.013	0.013
T/h-BN-bi	η^1	−0.034	0.034
	η^6	−0.030	0.030
BT/h-BN-bi	η^1	−0.039	0.039
	η^6	−0.038	0.038
DBT/h-BN-bi	η^1	−0.052	0.052
	η^6	−0.041	0.041

Author contributions

Zhengjian Hou: calculation performing, results analysis, writing and organization; Xufeng Lin: idea development, research funding provision, writing and organization; Ke Wu: discussion, writing; Hua Chi: discussion, writing; Wumin Zhang: discussion, revision; Lishuang Ma: funding provision, discussion; Yanyan Xi: discussion.

Conflicts of interest

There are no conflicts to declare.

Acknowledgements

Support from the National Natural Science Foundation of China (22003076, 21576291) and the Fundamental Research Funds for the Central Universities (23CX03007A, 22CX06012A) is gratefully acknowledged.

References

1 H. Li, H. Ran, Y. Li, N. Lv, J. Yin, J. Zhang, C. Wang, W. Jiang, W. Zhu, H. Li and H. Ji, *J. Environ. Chem. Eng.*, 2021, **9**, 105886–105899.
2 S. A. Ganiyu and S. A. Lateef, *Fuel*, 2021, **294**, 120273–120295.
3 Z. Chen, L. Ling, B. Wang, H. Fan, J. Shangguan and J. Mi, *Appl. Surf. Sci.*, 2016, **387**, 483–490.
4 A. Tanimu and K. Alhooshani, *Energy Fuels*, 2019, **33**, 2810–2838.
5 W. Jiang, H. Jia, H. Li, L. Zhu, R. Tao, W. Zhu, H. Li and S. Dai, *Green Chem.*, 2019, **21**, 3074–3080.
6 W. Jiang, K. Zhu, H. Li, L. Zhu, M. Hua, J. Xiao, C. Wang, Z. Yang, G. Chen, W. Zhu, H. Li and S. Dai, *Chem. Eng. J.*, 2020, **394**, 124831–124839.
7 R. Abro, A. A. Abdeltawab, S. S. Al-Deyab, G. Yu, A. B. Qazi, S. Gao and X. Chen, *RSC Adv.*, 2014, **4**, 35302–35317.
8 G. Mohebali and A. S. Ball, *Int. Biodeterior. Biodegrad.*, 2016, **110**, 163–180.
9 Y. Li, N. Lv, C. Wang, J. Zhang, W. Fu, J. Yin, H. Li, W. Zhu and H. Li, *J. Mol. Graph. Model.*, 2020, **101**, 107715–117725.
10 Y. X. Li, J. X. Shen, S. S. Peng, J. K. Zhang, J. Wu, X. Q. Liu and L. B. Sun, *Nat. Commun.*, 2020, **11**, 3206–3215.
11 T. Feng, Y. Wang, Y.-n. Wu, D. M. Kabtamu, K. László and F. Li, *J. Mater. Chem. A*, 2020, **8**, 8678–8683.
12 P. Tan, Y. Jiang, L.-B. Sun, X.-Q. Liu, K. AlBahily, U. Ravon and A. Vinu, *J. Mater. Chem. A*, 2018, **6**, 23978–24012.
13 R. Menzel, D. Iruretagoyena, Y. Wang, S. M. Bawaked, M. Mokhtar, S. A. Al-Thabaiti, S. N. Basahel and M. S. P. Shaffer, *Fuel*, 2016, **181**, 531–536.
14 R. Neubauer, M. Husmann, C. Weinlaender, N. Kienzl, E. Leitner and C. Hochenauer, *Chem. Eng. J.*, 2017, **309**, 840–849.
15 B. S. Crandall, J. Zhang, V. Stavila, M. D. Allendorf and Z. Li, *Ind. Eng. Chem. Res.*, 2019, **58**, 19322–19352.
16 R. Mahmoudi and C. Falamaki, *Fuel*, 2016, **173**, 277–284.
17 M. Moradi, R. Karimzadeh and E. S. Moosavi, *Fuel*, 2018, **217**, 467–477.
18 X. N. Li, S. S. Peng, L. N. Feng, S. Q. Lu, L. J. Ma and M. B. Yue, *Microporous Mesoporous Mater.*, 2018, **261**, 44–50.
19 N. A. Khan, J. W. Yoon, J. S. Chang and S. H. Jhung, *Chem. Comm.*, 2016, **52**, 8667–8670.
20 J.-X. Qin, P. Tan, Y. Jiang, X.-Q. Liu, Q.-X. He and L.-B. Sun, *Green Chem.*, 2016, **18**, 3210–3215.
21 J. Xiong, W. Zhu, H. Li, W. Ding, Y. Chao, P. Wu, S. Xun, M. Zhang and H. Li, *Green Chem.*, 2015, 1647–1656.
22 J. Xiong, L. Yang, Y. Chao, J. Pang, M. Zhang, W. Zhu and H. Li, *ACS Sustainable Chem. Eng.*, 2018, **6**(8), 9912–9920.
23 E. C. Anota, G. H. Cocoletzi and A. M. G. Tapia, *Open Chem.*, 2015, **13**, 734–742.
24 H. Ji, J. Sun, P. Wu, Y. Wu, J. He, Y. Chao, W. Zhu and H. Li, *Fuel*, 2018, **213**, 12–21.
25 P. Wu, Y. Wu, L. Chen, J. He, M. Hua, F. Zhu, X. Chu, J. Xiong, M. He, W. Zhu and H. Li, *Chem. Eng. J.*, 2020, **380**, 122526–122534.
26 E. C. Anota, *SN Appl. Sci.*, 2022, **4**, 295.
27 M. C. F. Bautista, D. Cortés-Arriagada, E. Shakerzadeh and E. C. Anota, *J. Mol. Liq.*, 2022, **355**, 118980.
28 H. Li, J. Zhang, J. Yi, J. Luo, S. Zhu, L. Sun, J. Xiong, W. Zhu and H. Li, *Chem. Eng. Res. Des.*, 2019, **144**, 11–18.
29 X.-L. Sun, Z. Liu and Z.-L. Cheng, *J. Alloys Compd.*, 2021, **885**, 160976–160988.
30 H. Li, Y. Zhang, N. Lv, J. Yin, J. Zhang, H. Ran, M. Zhang, W. Jiang, W. Zhu and H. Li, *J. Environ. Chem. Eng.*, 2021, **9**, 106463–106475.
31 H. T. Larijani, M. Jahanshahi, M. D. Ganji and M. H. Kiani, *Phys. Chem. Chem. Phys.*, 2017, **19**, 1896–1908.
32 H. Jouypazadeh and H. Farrokhpour, *J. Mol. Struct.*, 2018, **1164**, 227–238.
33 H. Li, C. Wang, S. Xun, J. He, W. Jiang, M. Zhang, W. Zhu and H. Li, *J. Mol. Graph. Model.*, 2018, **82**, 93–100.

34 Y. Sun, S. Gao, F. Lei and Y. Xie, *Chem. Soc. Rev.*, 2015, **44**, 623–636.
35 M. J. Frisch, G. W. Trucks, H. B. Schlegel, G. E. Scuseria, M. A. Robb, J. R. Cheeseman, G. Scalmani, V. Barone, B. Mennucci, G. A. Petersson, H. Nakatsuji, M. Caricato, X. Li, H. P. Hratchian, A. F. Izmaylov, J. Bloino, G. Zheng, J. L. Sonnenberg, M. Hada, M. Ehara, K. Toyota, R. Fukuda, J. Hasegawa, M. Ishida, T. Nakajima, Y. Honda, O. Kitao, H. Nakai, T. Vreven, J. A. Montgomery Jr, J. E. Peralta, F. Ogliaro, M. Bearpark, J. J. Heyd, E. Brothers, K. N. Kudin, V. N. Staroverov, R. Kobayashi, J. Normand, K. Raghavachari, A. Rendell, J. C. Burant, S. S. Iyengar, J. Tomasi, M. Cossi, N. Rega, J. M. Millam, M. Klene, J. E. Knox, J. B. Cross, V. Bakken, C. Adamo, J. Jaramillo, R. Gomperts, R. E. Stratmann, O. Yazyev, A. J. Austin, R. Cammi, C. Pomelli, J. W. Ochterski, R. L. Martin, K. Morokuma, V. G. Zakrzewski, G. A. Voth, P. Salvador, J. J. Dannenberg, S. Dapprich, A. D. Daniels, Ö. Farkas, J. B. Foresman, J. V. Ortiz, J. Cioslowski and D. J. Fox, *Gaussian 09, revision D.01*, Gaussian Inc., Wallingford, CT, 2013.
36 K. M. Eid and H. Y. Ammar, *Appl. Surf. Sci.*, 2011, **257**, 6049–6058.
37 J. Beheshtian, A. A. Peyghan and Z. Bagheri, *Appl. Surf. Sci.*, 2012, **258**, 8171–8176.
38 J. Beheshtian, A. A. Peyghan, M. B. Tabar and Z. Bagheri, *Appl. Surf. Sci.*, 2013, **266**, 182–187.
39 G. I. Csonka, *J. Mol. Struct. Theochem.*, 2002, **584**, 1–4.
40 S. Grimme, *J. Comput. Chem.*, 2011, **32**, 1456–1465.
41 Y. X. Yu, *J. Mater. Chem. A*, 2014, **2**, 8910–8917.
42 J. Li, H. Gan, Y. Xu, C. Wang, Y. Pei, F. L. Gu and G. Wang, *CrystEngComm*, 2018, **20**, 6775–6785.
43 M. A. Spackman and A. S. Mitchell, *Phys. Chem. Chem. Phys.*, 2001, **3**, 1518–1523.
44 D. G. A. Smith, L. A. Burns, A. C. Simmonett, R. M. Parrish, M. C. Schieber, R. Galvelis, P. Kraus, H. Kruse, R. Di Remigio, A. Alenaizan, A. M. James, S. Lehtola, J. P. Misiewicz, M. Scheurer, R. A. Shaw, J. B. Schriber, Y. Xie, Z. L. Glick, D. A. Sirianni, J. S. O'Brien, J. M. Waldrop, A. Kumar, E. G. Hohenstein, B. P. Pritchard, B. R. Brooks, H. F. Schaefer III, A. Yu. Sokolov, K. Patkowski, A. E. DePrince III, U. Bozkaya, R. A. King, F. A. Evangelista, J. M. Turney, T. D. Crawford and C. D. Sherrill, *J. Chem. Phys.*, 2020, **152**, 184108.
45 T. Lu and F. Chen, *J. Comput. Chem.*, 2012, **33**, 580–592.
46 W. Humphrey, A. Dalke and K. Schulten, VMD – visual molecular dynamics, *J. Mol. Graphics*, 1996, **14.1**, 33–38.
47 U. Paliwal, G. Sharma and K. B. Joshi, *Mater. Today Proc.*, 2022, **50**, 301–306.
48 O. Karalti, D. Alfe, M. J. Gillan and K. D. Jordan, *Phys. Chem. Chem. Phys.*, 2012, **14**, 7846–7853.
49 J. G. McDaniel, K. Yu and J. R. Schmidt, *J. Phys. Chem. C*, 2012, **116**, 1892–1903.